International Journal of Chemical Engineering

Materials and Corrosion Advancements

Lead Guest Editor: Oluranti Agboola
Guest Editors: Ojo Sunday Fayomi and Emmanuel Rotimi Sadiku

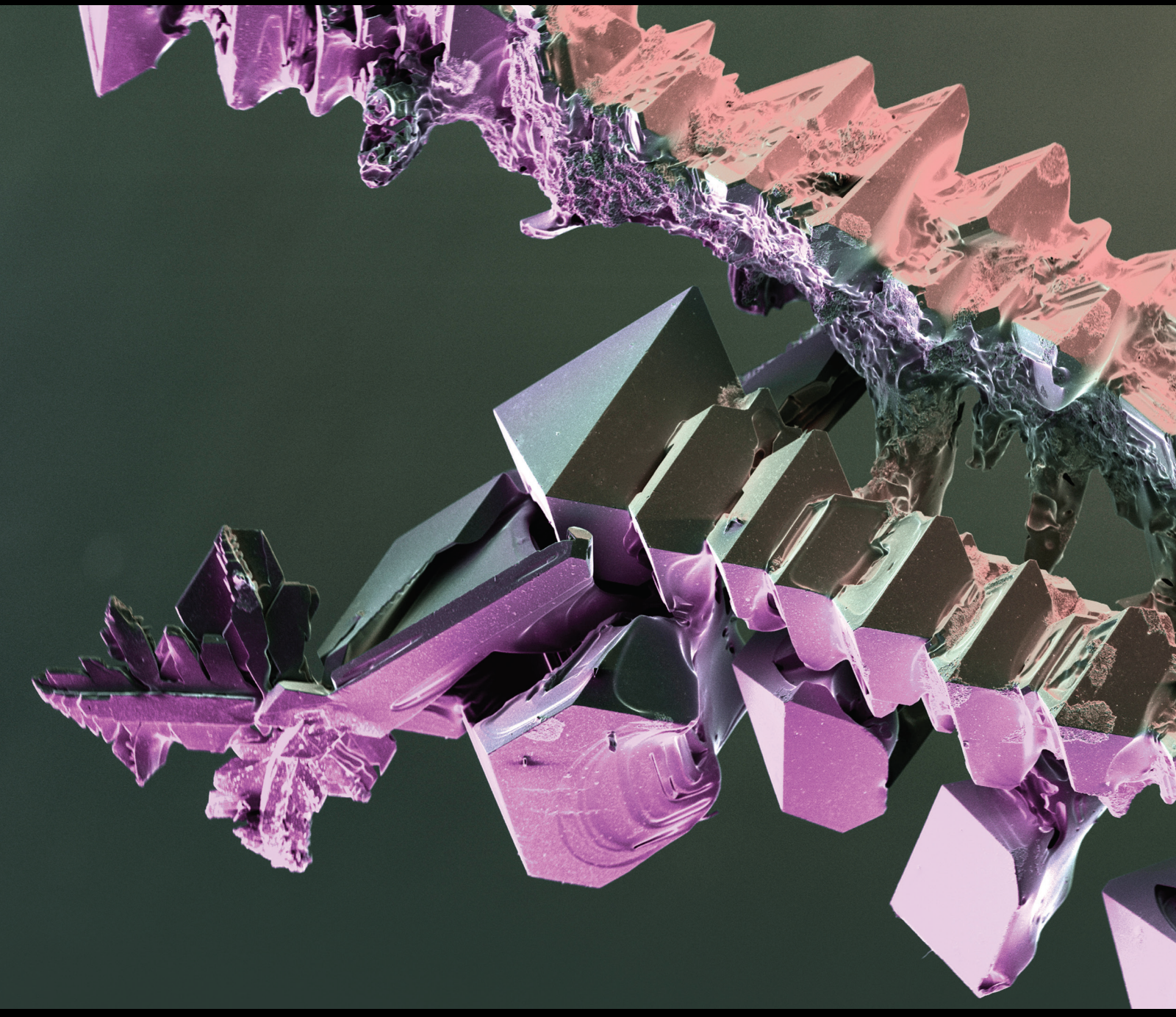

Materials and Corrosion Advancements

International Journal of Chemical Engineering

Materials and Corrosion Advancements

Lead Guest Editor: Oluranti Agboola
Guest Editors: Ojo Sunday Fayomi and Emmanuel Rotimi Sadiku

Contents

Hindawi
International Journal of Chemical Engineering
Volume 2021, Article ID 8871228, 8 pages
https://doi.org/10.1155/2021/8871228

Research Article

The Production of Zeolite Y Catalyst From Palm Kernel Shell for Fluid Catalytic Cracking Unit

Angela Mamudu,[1] **Moses Emetere**,[2] **Felix Ishola**,[3] **and Dorcas Lawal**[1]

[1]*Department of Chemical Engineering, Covenant University, Ota, Nigeria*
[2]*Department of Physics, Covenant University, Ota, Nigeria*
[3]*Department of Mechanical Engineering, Covenant University, Ota, Nigeria*

Correspondence should be addressed to Angela Mamudu; angela.mamudu@covenantuniversity.edu.ng

Received 15 June 2020; Revised 15 September 2020; Accepted 17 March 2021; Published 31 March 2021

Academic Editor: Ho SoonMin

Exorbitant costs of fluid catalytic cracking unit (FCCU) catalysts coupled with their ever-increasing demand have led researchers to develop alternative materials from indigenous sources. In this study, the zeolite Y component of the FCCU catalyst was synthesized from palm kernel shells. Leaching was carried out with the aid of citric acid to remove impurities. The synthesis process was done using alkaline hydrothermal treatment while varying reagent concentration and reaction time. The resultant products were characterized using XRF, XRD, FTIR, BET, and SEM analysis. The XRD and XRF showed a high silicate content level, while an 85% reduction in iron oxide impurities was observed after leaching. The process carried out at a duration of 9 hours, a temperature of 80°C with a NaOH molarity strength of 2 mol/L, had the highest SiO2 and Si/Al ratio value. A spongy, porous zeolite crystal was formed with the presence of hydroxyls in its sodalite cage. All samples had a combination of types II & I adsorption isotherms, Si/Al ratio of 2–5, and specific surface area within 80–260 m^2/g, which indicates the presence of intermediate mesostructured Zeolite Y catalyst. Synthesized zeolite Y showed a more significant gap in its structural formation as the addition of NaOH decreased the grain size by 14.3%. FTIR highlighted the significant functional groups present in the novel compound, which, when compared to previous works, proves its suitability.

1. Introduction

Petroleum refining is a process through which crude oil is converted into useful products [1]. Although it has many distinct units, the conversion and separation units always play significant roles [2]. The fluid catalytic cracking unit (FFCU), which falls under the conversion group, remains an indispensable unit operating in refineries. It converts about 40% of the heavy residues gotten from both vacuum and atmospheric distillation into lighter and more useful products with higher octane values [3, 4]. According to Vogt and Weckhuysen [5]; the heavy hydrocarbon molecules (majorly gas oil) preheated at about 149°C are charged as a feedstock into a catalyst riser containing particles of powdered catalyst that are fluidized by the hydrocarbon vapors. Cracking occurs within 2–4 seconds in the riser, where the heavy molecules are broken down into lighter and shorter chain molecules at 1 atm with a temperature range of 520°C–550°C. Separation occurs in the distillation column while the catalyst particles are re-generated.

One of the significant achievements that have contributed to the ever-growing popularity of the FCCU has been the introduction of Zeolite catalysts. Zeolites are hydrated alumina silicate materials made from inter-linked tetrahedral of alumina (AlO_4) and silica (SiO_4). 130 out of 840 catalysts used in industrial applications are based on zeolites, and the FCCU in petroleum refineries utilizes over 61% of these zeolite-based catalysts. The zeolite component makes up 10–50 wt.% of the catalyst and provides activity, stability, and selectivity. Zeolites are produced both synthetically and naturally, but most of the zeolites used in the FCCU are synthetically produced. Synthetic zeolite has fewer

impurities and has a more uniform pore size than its natural counterparts [6]. However, various types of synthetic zeolite's major catalyst exist. Zeolite Y from the faujasite family has continued to gain worldwide recognition, mainly due to its inherent properties-acidity, thermal stability, and the increase in gasoline yield [7].

Zeolites have a substantial global consumption of nearly 4 million metric tons per annum, while commercial catalyst keeps experiencing unprecedented inflation [8]. The chemicals used in the conventional synthesis of commercial zeolites are very costly, leading to high zeolite production costs [9]. Also, most of the natural zeolites are gotten through mining, and frequent mining can result in environmental degradation. Therefore, there is a need to provide alternate materials from indigenous sources that are less expensive and environmentally friendly. Researchers in the past have tried to investigate the suitability of various indigenous sources (fly ash, natural clays, rice husks, oil palm ash) for zeolite Y synthesis. Results show a reasonable amount of silicon compounds present in them, a prerequisite for zeolite synthesis [10]. Ariffin [11] proved that silica and alumina are significant components in producing zeolites from oil palm ash. Faizul et al. [12] ascertained the effectiveness of citric acid used in the leaching treatment to extract silica from oil palm ash.

Although various research has been carried out on palm kernel shell's total utilization, none is channeled to the fluid catalytic cracking unit. Hence, this study ascertains Zeolite Y catalyst production from palm kernel shells via pre-treatment, hydrothermal, and various characterization processes. Pre-treatment involves ashing, which extracts silica contents from the feed while leaching further removes metallic oxide impurities. The effects of varying reagent concentration and reaction time during the hydrothermal process were also observed for optimum production. Physicochemical properties of selected samples were analyzed via X-ray Fluorescence (XRF), X-ray Diffraction (XRD), Brunaurer-Emmett Teller (BET), Scanning Election Microscope (SEM), and Fourier Transform Infrared Spectroscopy (FTIR) to determine its suitability for use in the fluid catalytic cracking unit of a refinery.

1.1. Palm Kernel Shells. Palm kernel shells (PKS) are waste products from oil palm processing [13]. They are generally the remains after palm kernel nuts are crushed in oil palm mills. A combination of Tenera and Dura (oil palm variety) was used in this study since it was difficult to separate the two. Although the literature on using palm kernel shells in zeolite synthesis has not been extensive, its maximization in other areas has been highlighted. Palm kernel shells can be used to produce biomass briquettes, activated carbon, and secondary fuel for boilers [14, 15]. Therefore, using palm kernel shells as a starting material in zeolite production is driven by low cost and availability in large quantities. The process will also serve as a means of effective utilization of waste.

Generally, the synthesis of solid-state materials can either take place in a solid-state or the presence of a liquid solvent [16]. The solid-state method usually requires a high temperature above 300°C to overcome difficulties transporting the reactants to the reaction sites. Synthesis of zeolite Y catalyst occurs via molecular transport in the liquid phase since it is much easier (>300°C). The alkaline hydrothermal approach was adopted for this process to ensure the crystallization of molecular sieve zeolite. The process was achieved by mixing an aluminate and silicate source to form amorphous aluminosilicate gel. The crystallization process involves nucleation and crystal growth. Nucleation involves creating the smallest entity, which can be recognized as having a crystalline atomic structure. Simultaneously, crystal growth ensures the nuclei's evolution to larger macroscopic sizes [17].

The Zeolite Y catalyst prices in the Fluid Catalytic Cracking unit generally vary based on the Si/Al ratio. Presently top producers/suppliers (Jiangsu AFNANO Materials Tech Co., Ltd and Xiamen Futt Laboratory Materials Limited) sell 100–499 grams (US$ 0.26–0.30); 500–999 grams (the US $0.26) and ≥1000 grams (the US $0.26) [18]. All works carried out on the synthesis of Zeolite Y catalyst from palm kernel shell ash, fly ash, or industrial clays has been carried out on a laboratory scale to prove the feasibility of the process [11, 19–26] and [27].

2. Material and Methods

The methods adopted to accomplish the research focus are presented in the flowchart below (Figure 1).

2.1. Preparation of Raw Materials. The Palm Kernel Shells used were sourced from two locations (Ikere and Sekona District) in Ogun State, Nigeria. These materials were first washed to remove sand and other dirt. Afterward, they were sundried for five days to remove moisture. The dried shells were then crushed with a mechanical grinder to a particle size of 75–100 micrometers. Calcination of the crushed palm kernel shells was carried out in a Barnstead box-type high-temperature muffle furnace (F46118) at a temperature of 800°C for three hours to yield palm ash. F46118 operates with 240 volts, 40 amps while the maximum ramp rates for heat up are: 100°C per minute from 25°C to 1000°C and 15°C per minute from 1000°C to 1700°C.

2.2. Leaching Process. The leaching process was carried out using the method reported by Faizul et al. [12]. This method replaced the conventional use of strong acids in leaching treatment with citric acid because of its environmentally friendly nature. The leaching treatment was carried out to remove metallic oxide impurities present in the PKSA so that more of the silica can be utilized for zeolite synthesis. 20 g of PKSA was put into a 500 ml citric acid solution in a beaker, placed on the hot plate (temperature set at 70°C) for 60 minutes. The PKSA was rinsed with distilled water at room temperature to remove citric acid content from the ash. Drying was carried out at a temperature of about 70°C for 55 minutes in the oven and combustion at 800°C for 30 minutes in the tube furnace. The chemical composition of the treated ash was determined by X-ray fluorescence spectroscopy (XRF).

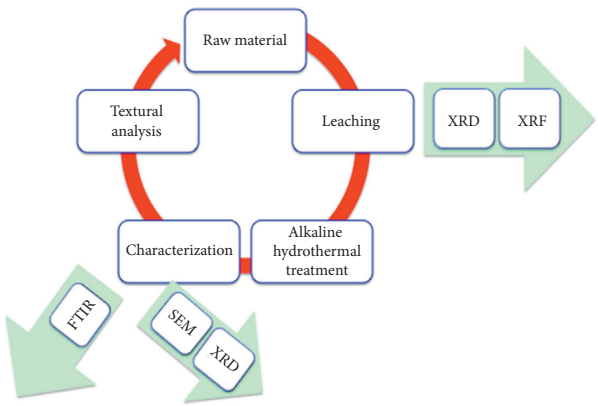

Figure 1: Flow chart for process methods.

2.3. Alkaline Hydrothermal Treatment. The hydrothermal-treatment procedure was adopted from Faizul et al. [21] and Faizul and Abdullah [20] with some modifications. The alkaline hydrothermal treatment is an essential one because it mimics the set conditions of zeolite minerals' formation in nature [28]. Different NaOH concentrations (1M, 2M, and 3M) were reacted with a known weight of treated PKSA with a ratio of 1 : 0.3. The mixture was then aged and crystallized with mechanical agitation placed in a water bath. The synthesis was carried out at a temperature of 80°C and at different reaction times (5, 7, and 9 hours). Reliable products obtained from the alkaline hydrothermal treatment were recovered by filtration and washed with distilled water. Recovered products were then dried at 70°C for 30 minutes and cooled in a desiccator before product characterization-XRD, FTIR, XRF, BET, and SEM analysis.

2.4. Product Characterization. XRF remains a non-destructive analytical technique carried out on the raw palm kernel ash, treated palm kernel ash, and synthesized product to determine the materials' elemental composition. The XRF was carried out using model TEFA ORTE, copper K-alpha with a wavelength of 1.550 radiation, operating at 40 kV (kilovolts) and 25 mA (milliampere). X-Ray Diffractometer (XRD) analysis is generally used to study the crystallographic structure, chemical composition, and physical properties of materials. The calcined PKSA were analyzed using a Rigaku Rotaflex 200B diffractometer equipped with copper K-alpha with a wavelength of 1.54056 radiation. It was operated at 40 kV (kilovolts) and 40 mA (milliampere). XRF identifies elemental percentages of crystallinity in a material. SEM was done with model Schottky Field Emission JSM–760°F on the treated palm ash and synthesized product to determine the microstructures. However, the microstructure reveals its morphology, composition, and particle surface crystallography information. The FTIR analysis was carried out on the product to identify any form of organic, polymeric, and inorganic materials present.

2.5. Textural Properties. The synthesized zeolite's efficiency from palm kernel shell ash (PKSA) depends mainly on its textural properties, including the specific surface area and pore size distribution. During the production of PKSA, two steps are involved-the raw shells' carbonization to enrich the carbon content and the carbonized shells' activation. The activation process frees deposited tars and decomposed products from initially blocked pores. Therefore, the level of porosity achieved mainly depends on the mechanism of carbon removal, which is chiefly controlled by the activating conditions (reagent concentration and reaction time). In this study, Physisorption of nitrogen (77 k) at relatively low pressure (10^{-6} P/Po) for all active carbon is employed. The micropore volume was measured using the Dubinin-Radushkevich (DR) theory, associated with enhanced adsorbent–adsorbate interactions [29]. The adsorption isotherms were interpreted by applying the modified BET (Brunauer–Emmett–Teller) method.

3. Results and Discussion

3.1. Characterization of PKSA and Treated PKSA. The initial and treated PKSA were both characterized using X-ray fluorescence to compare the percentage of impurities in both samples and determine the leaching treatment's effectiveness. Table 1 shows the weight percentage of significant constituents found in both crude and treated PKSA.

Generally, variation in chemical composition can be traced to geographical location and soil type [30]. It is observed from Table 1, row 4 above, that there has been a significant increase in the silica content of the oil palm ash and a reduction (85%) in the metallic oxides (impurities) after the leaching treatment, which proves that the leaching treatment was effective. The citric acid contains carboxyl groups that behave as a chelating agent, reacting with metallic ions to form stable complexes, which resulted in the removal of metallic ions [12]. Table 1 also affirms the findings of Iskander et al. [31] that the desorption pattern of the metallic impurities varies in the zeolite.

3.2. Characterization of Synthesized Zeolite

3.2.1. XRF Analysis. As stated earlier, the synthesis of zeolite Y from the oil palm ash by a hydrothermal treatment was carried out at different NaOH concentrations (2 M and 3 M) and different reaction times (5, 7 and 9 hours) to observe the effect of these variations on the composition of the produced Zeolite Y. The reaction temperature was, however, fixed at 80°C. Table 2 presents the results of the XRF analysis of the synthesized Zeolite Y catalysts showing the composition of the major constituents. All the synthesized zeolite Y samples appear to have a significant silicon dioxide and aluminum oxide component with a relatively high iron oxide percentage. It can also be observed from Table 2 that the composition of SiO_2 and Al_2O_3 compared to other constituents were generally higher across all samples. As shown in Table 2, the phenomenon also corresponds to the work carried out by Ariffin [11]. The highest composition of SiO_2 reached was at 2 M and 9 hours, suggesting that concentration and reaction time significantly affect the chemical composition of synthesized zeolite.

Table 1: Chemical composition of PKSA and leached PKSA.

Chemical constituent	PKSA (%)	Treated PKSA (%)
SiO_2	42.0	50.7
Al_2O_3	6.9	4.6
Fe_2O_3	2.5	0.3
MnO	0.3	0.6
CaO	12.0	14.1
Others	36.3	29.8

Others include P_2O_5, K_2O, TiO_2, MgO, and Na_2O.

Table 2: Chemical Composition of Synthesized Zeolite Y under varying Conditions.

Constituent	2 M/5 hours	2 M/7 hours	2 M/9 hours	3 M/5 hours	3 M/7 hours	3 M/9 hours
SiO_2	57.20	52.70	57.38	52.21	53.71	54.37
Al_2O_3	23.20	30.95	23.22	28.60	30.94	28.35
Fe_2O_3	0.03	0.20	0.03	0.02	0.20	0.03
MnO	0.14	0.08	0.12	0.11	0.02	0.07
CaO	6.15	8.12	6.18	9.45	8.15	7.22
Others	13.28	7.95	13.07	9.61	6.98	9.96

Others include P_2O_5, K_2O, TiO_2, MgO, and Na_2O. Values in percentage.

Measure of acidity. Generally, the acidity of a given catalyst is a measure of how fast a reaction can proceed in the catalyst's presence. Usually, zeolite catalysts experience chemical changes during cracking reactions, and as a result, their activity as a function of time becomes lower, hence the need for regeneration [24]. The Si/Al ratio of a zeolite catalyst usually determines its acidity. The acidity tends to increase in strength with an increasing Si/Al ratio. Although the Si/Al ratio increases, the cation concentration and ion exchange capacity decrease [32]. Table 3 shows the Si/Al ratio (SAR) of the starting material for zeolite synthesis and the synthesized zeolite samples. It can be observed from the table that the Si/Al ratio of the synthesized Zeolites was higher than the ratio for the treated ash.

Generally low (1–1.5 Si/Al ratio) and intermediate zeolites (2–5 Si/Al ratio) can comfortably remove water from organics and carry out separation and catalysis on dry streams. High zeolite (10–100 Si/Al ratio) is hydrophobic can recover organics from the water stream and carry out separations and catalysis in the presence of water [32]. The Si/Al ratio variation also produces differences in the Si–O–Al group's amount and distribution in their crystal structure. Hence, changes in the Si/Al ratio result in the alteration of the zeolite crystal structure, which plays a significant role in determining zeolites' behavior or properties [33].

Although sample 2 M/80°C/9 hours has the most considerable value (2.18), samples 2 M/5 hours, 3 M/5 hours and 3 M/80°C/9 hours also fell within the range of 2–5, which agrees with the literature value of intermediate zeolite Y catalyst [7]. The thermal and hydrothermal stabilities of zeolite are strongly related to its Si/Al ratio. Hence these values depict that the synthesized zeolites have high thermal stability, which is required for a fluid catalytic cracking catalyst [34].

Table 3: Si/Al ratio of Synthesized and Leached Samples.

Samples	Si/Al
2 M/80/5 hours	2.16
2 M/80/7 hours	1.42
2 M/80/9 hours	2.18
3 M/80/5 hours	2.0
3 M/80/7 hours	1.42
3 M/80/9 hours	2.0
Treated ash	1.18

3.2.2. SEM Analysis. Figure 2 shows the morphology of the treated palm ash and synthesized zeolite Y. Figure 2(b) depicts the underdeveloped zeolite Y crystals, which are gradually being formed. The underdeveloped nature of the zeolite crystals is attributed to the reaction conditions. This zeolite Y sample was initially synthesized using a reagent concentration of 2 M and a reaction time of 9 hours. Increasing the aging time and concentration (3 M and a reaction time of 9 hours) would promote a more defined structure, as seen in Figure 2(c). This representation presents a more defined crystal structure. It shows a complex three-dimensional, highly porous spongy crystalline zeolite, which agrees with a standardized zeolite Y catalyst [35]; Chindaprasirt et al. [36] and [25]. However, the crystals have a small surface area primarily due to a composite formed containing few zeolite crystals and non-crystallization palm kernel shells. It is also caused by the coalescence of neighboring micro-pores and pore capillaries' breakage in increased internal surface exposure [37–39]. The crystals' size could also mean insufficient aging time, resulting in the partial formation of crystalline zeolite Y.

3.2.3. Structural Analysis of Synthesized Zeolite Catalyst. In this section, the leaching process's structural effect and the alkaline hydrothermal treatment on the palm kernel ash were carried using computational processing of the scanning electron microscopy images. The 3D structural display of the background content, as shown in Figure 3, describes the tendencies of the cation exchange capacity of the material. The 3D structural display also determines the number of significant disjointed gaps, also known as grain size. Due to the higher grain size (244 nm) of the leached palm kernel ash compared to that of the synthesized zeolite Y catalyst (209.334 nm), it is believed to have more significant gaps in its structural formation within a thickness of 0.61 μm. The leached palm ash has a compact arrangement of its particles within a thickness of 0.24 μm, which means fewer structural formation gaps. The addition of sodium hydroxide also decreased the grain size by 14.3%.

3.2.4. Fourier Transform Infrared Spectroscopy Analysis. An FTIR Spectrophotometer was used to show the vibrational spectroscopy of zeolite Y, as observed in Figure 4 below. The spectra show strong IR absorption in the spectral region below 1200 cm^{-1}. Vibration frequencies of the zeolite lattice result from stretching and bending modes of the T-O units. This is observed in the range 300 to 1300 cm^{-1} which indicates the presence of SiO_4 or $A1O_4$. The crystallization of

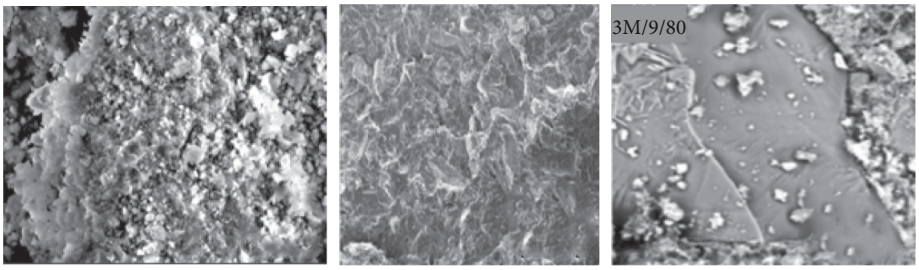

(a) (b) (c)

Figure 2: Representative SEM image of (a) Leached Palm Ash (b) Synthesized Zeolite Y IM/9 Hours (c) Synthesized Zeolite Y -3 M/9 Hours. All images were taken at a pressure of 70 pa, accelerating voltage of 15 kV, working distance of 10.8 mm, lens magnitude of 15000x, and horizontal field width of 124 μm.

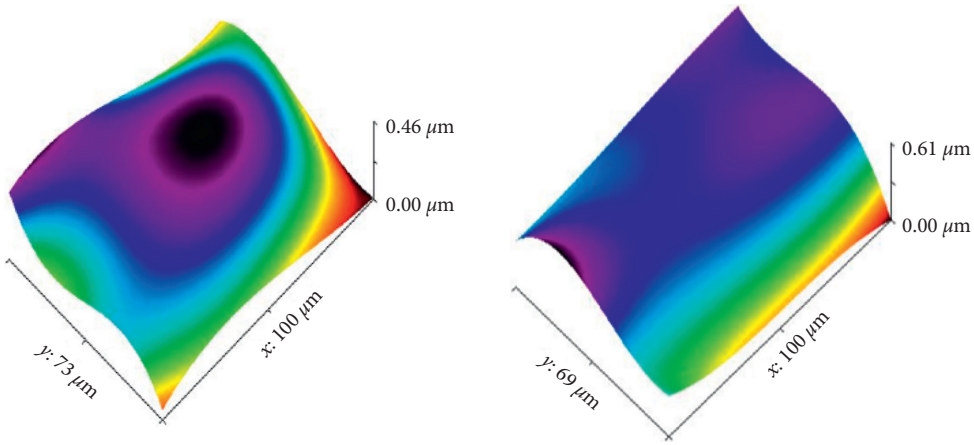

(a) (b)

Figure 3: Structural analysis of (a) leached palm ash (b) synthesized zeolite Y.

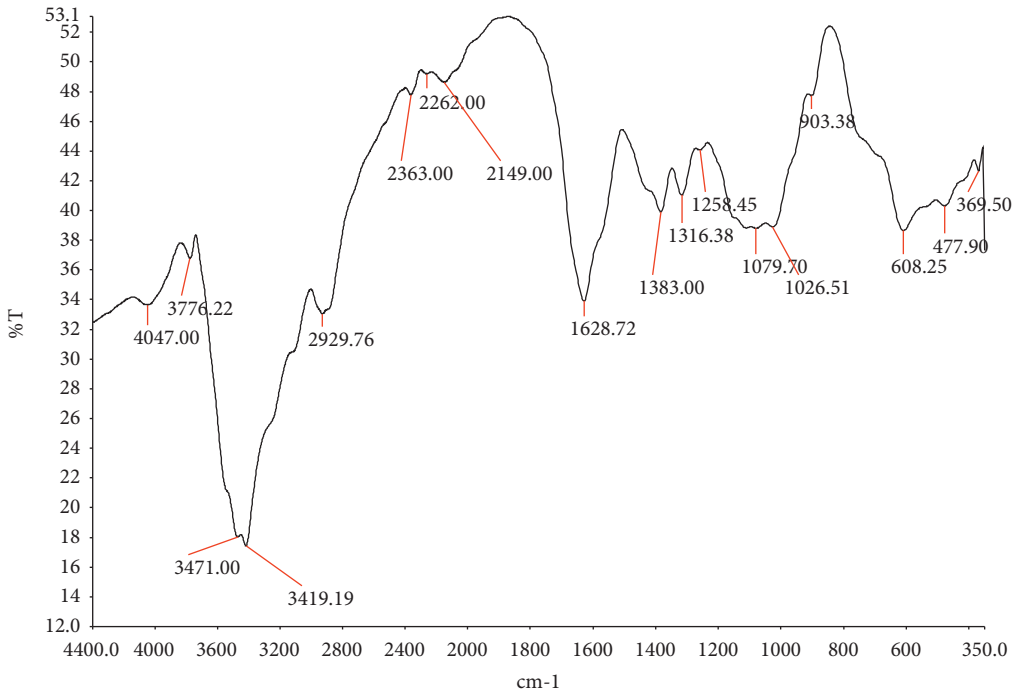

Figure 4: FTIR spectra of synthesized zeolite Y.

pure zeolite Y using silica is favored at a temperature lower than 100°C, with less Na_2O or higher SiO_2 content in the initial mixture. This is because zeolite Y is highly reactive due to the ability of its iron exchange forms to produce hydroxyl radicals from H_2O_2 [10]. OH, bands are single intense bands occurring at approximately 3419 and 3471 cm^{-1}, respectively.

These bands are accredited to the presence of hydroxyls in the faujasite super-cage. The faujasite super-cage usually consists of sodalite cages as its building block; hence its presence is depicted in the FTIR spectra [25, 35]. The FTIR spectrum also showed medium bands at 1628 cm^{-1}. These bands can be attributed to the H_2O deformation mode, usually seen at 1659 cm^{-1}. The peak at about 1600 cm^{-1} points to water molecules, which shows that complete dehydration has not been achieved for the zeolite samples. The FTIR spectra of the synthesized Zeolite Y in this study are like those obtained from past works. [40, 41]. This further proves Zeolite Y's suitability synthesized from palm kernel shells to substitute commercial Zeolite Y catalysts in the FCCU. The impurities noticed are likely oxides, as shown in [31, 37, 39].

3.2.5. XRD Analysis. The XRD for the calcined palm kernel (PK) shell and the zeolite are presented in Figure 5. As shown in Figure 5 below, the prominent peaks that were present at 600°C for palm kernel ashes were muscovite (M), quartz (Q), and hematite (H). However, the quartz peaks showed a higher diffused pattern-an indication of high silicate content. Muscovite $kAl_2(Si_3AlO_{10})(OH)_2$ and hematite (Fe_2O_3) also corresponds to data gotten from the XRF analysis. The peaks in the processed zeolite were found to correspond to the peaks of the quartz and hematite. It was observed that an unnamed peak in the calcined PK shell corresponds to one of the peaks in the zeolite. This unnamed peak may be impurity inherent in the palm kernel shell. The crystallographic information shows that the crystallinity of zeolite lies on planes (331), (533), (642), (664), and (840). The merged peaks of zeolite and quartz at (511) and (642) show that the raw material's crystallinity is almost unaltered despite the treatment. Therefore, the XRD result corroborated the high silicon content, as shown in Table 1.

3.2.6. Textural Properties of Synthesized Zeolite Y Catalyst and the Effect of Reagent Concentration and Reaction Time on Meso-Porosity of Synthesized Zeolite Y Catalyst. The volume filling of available micro-pores occurs because of the pore size's commensurability with the nitrogen molecules [42]. From Figure 6, it is observed that the isotherms of treated PKSA, 2 M/7/80, 2 M/5/80, and 3 M/9/80 is a combination of types II and I adsorption Isotherms accompanied by a prominent hysteresis of type H4 (according to the IUPAC classification of hysteresis loops) in between the region 0.04–0.08 P/Po. The isotherms and

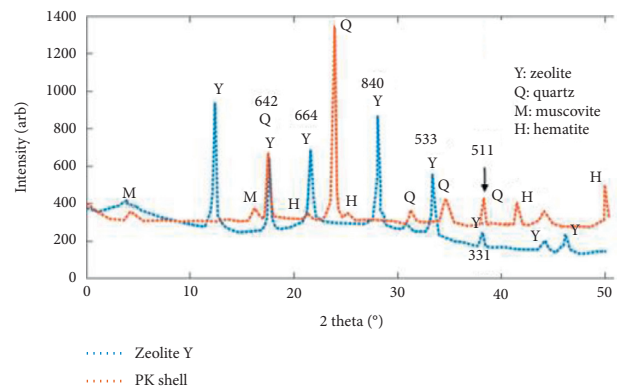

Figure 5: XRD for calcined palm kernel shell and zeolite.

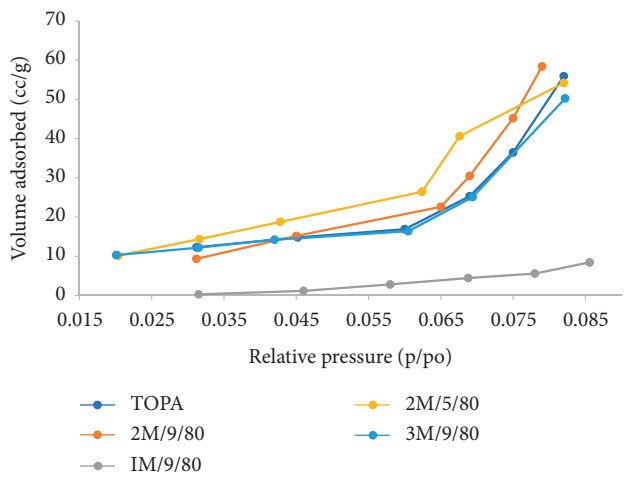

Figure 6: Relative pressure versus volume adsorbed for synthesized zeolite Y samples.

relative pressure values fall within standards for zeolite Y catalyst, as Yates [43] highlighted. These values also indicate a higher level of mesoporosity when compared to 1 M/9/80. These differences are primarily due to the nature of raw materials and the differences in treatment parameters [44].

These micro-pores are associated with the pore deepening mechanism, resulting in the steady increase of Brunauer–Emmett–Teller (BET) specific surface areas. The void fraction constitutes these micro-pores between graphitic layers with the restricted diameter, as shown in Figure 7. The specific surface areas of the samples were determined from N2 adsorption isotherms using a BET method. These values fall within the range of 80–260 m^2/g, which remains a prominent characteristic of mesostructured Zeolite Y catalyst [45]. Although the BET surface area is a useful indication; however, it should not be regarded as the actual surface area of a highly microporous material [46].

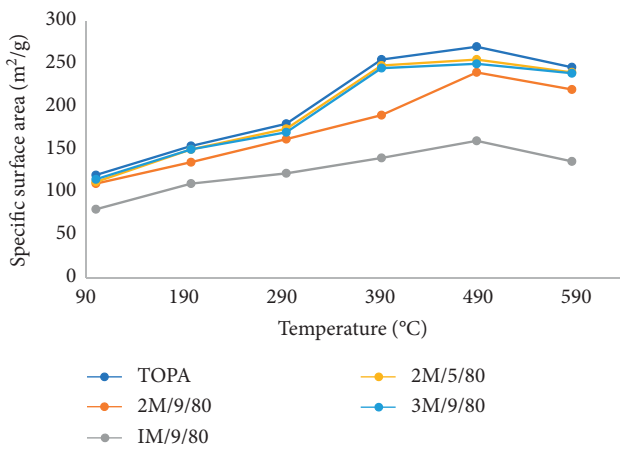

Figure 7: Temperature versus specific surface area for synthesized zeolite Y samples.

4. Conclusion

A spongy, porous zeolite crystal was formed with the presence of hydroxyls in its sodalite cage. All samples had a combination of types II & I adsorption isotherms, Si/Al ratio of 2–5, and specific surface area within 80–260 m^2/g, which indicates the presence of intermediate mesostructured Zeolite Y catalyst. FTIR highlighted the significant functional groups present in the novel compound, which proves its suitability for use in a fluid catalytic cracking unit.

Data Availability

Included within the article.

Conflicts of Interest

The authors declare that they have no conflicts of interest.

Acknowledgments

The authors want to express gratitude to the management of Covenant University, Nigeria, for providing an enabling environment for this research.

References

[1] A. O. Mamudu, E. Okonkwo, S. I. Okocha, E. E. Okoro, F. Elehinafe, and K. Igwilo, "The design of an integrated crude oil distillation column with submerged combustion technology," *The Open Chemical Engineering Journal*, vol. 13, no. 1, pp. 7–22, 2019.

[2] S. Haridoss, "A study on the role of catalysts used in catalytic cracking process in petroleum refining," *International Journal of Chemistry*, vol. 10, no. 7, pp. 79–86, 2017.

[3] M. E. Emetere, O. A. Mamudu, F. Ishola, D. Lawal, F. B. Elehinafe, and A. Odunayo, "The production of the matrix component of the fluid catalytic cracking unit from watermelon peel," *International Journal of Engineering and Technical Research*, vol. 9, no. 5, pp. 1259–1262, 2020.

[4] M. A. Fahim, T. A. Alsahhaf, and A. Elkilani, *Product Blending in Fundamentals of Petroleum Refining*, pp. 237–261, Elsevier, Amsterdam, Netherlands, 2010.

[5] E. T. C. Vogt and B. M. Weckhuysen, "Fluid catalytic cracking: recent developments on the grand old lady of zeolite catalysis," *Chemical Society Reviews*, vol. 44, no. 20, p. 7342, 2015.

[6] R. M. Barrer, *Hydrothermal Chemistry of Zeolites*, p. 360, Academic Press, New York, NY, USA, 1982.

[7] Z. Liu, C. Shi, D. Wu, S. He, and B. Ren, "A simple method of preparation of high silica zeolite Y and its performance in the catalytic cracking of cumene," *Journal of Nanotechnology*, vol. 2016, no. 7, pp. 1–6, 2016.

[8] W. Vermeiren and J.-P. Gilson, "Impact of zeolites on the petroleum and petrochemical industry," *Topics in Catalysis*, vol. 52, no. 9, pp. 1131–1161, 2009.

[9] Y. Yaping, Z. Xiaoqiang, Q. Weilan, and W. Mingwen, "Synthesis of pure zeolites from supersaturated silicon and aluminum alkali extracts from fused coal fly ash," *Fuel*, vol. 87, no. 10-11, pp. 1880–1886, 2008.

[10] M. M. Rahman and N. Hasnida, "Preparation of zeolite Y using local raw material rice husk as a silica source," *Journal of Scientific Research*, vol. 1, no. 2, pp. 285–291, 2009.

[11] B. A. Ariffin, "Production of zeolites from oil palm ash," Bachelor of Chemical Engineering Thesis, Universiti Malaysia Pahang, Gambang, Malaysia, 2010.

[12] C. P. Faizul, C. Abdullah, and B. Fazlul, "Extraction of silica from palm ash via citric acid," *Advances In Environmental Biology*, vol. 795, no. 12, pp. 3690–3695, 2013.

[13] F. Ishola, O. Towoju, A. Mamudu, O. Olatunji, S. Akinlabi, and J. Oladejo, "Nigerian oil palm industry as a sustainable renewable energy resource," in *E3S Web of Conferences*vol. 152, p. 02005, EDP Sciences, Les Ulis, France, 2020.

[14] F. Ishola, F. A. Oyawale, A. O. Inegbenebor, and H. O. Boyo, "Design of a high-temperature anaerobic gas-furnace suitable for pyrolysis," *IOP Conference Series Material Science Engineering*, vol. 413, 2018.

[15] N. Sabzoi, S. Siddhartha, A. Saadia, S. A. Brahim, and A. S. Muhammad, "A critical analysis on palm kernel shell from oil palm industry as a feedstock for solid char production," *Reviews in Chemical Engineering*, vol. 32, no. 5, pp. 489–505, 2016, eISSN 2191-0235, ISSN 0167-8299.

[16] J. Cejka, A. Corma, and S. Zone, *Zeolites and Catalysis: Synthesis, Reactions, and Applications*, Wiley-VCH, Weinheim, Germany, 2010.

[17] S. Gonthier and R. W. Thompson, "Effects of seeding on zeolite crystallisation, and the growth behavior of seeds," *Advanced Zeolite Science and Applications*, vol. 85, pp. 43–73, 1994.

[18] Alibaba.com, *Zeolite Y Catalyst*, Alibaba.com, Hangzhou, China, 2020, https://www.alibaba.com/showroom/zeolite+y+catalyst.html?fsb=y&IndexArea=product_en&CatId=&SearchText=zeolite+y+catalyst&isGalleryList=G.

[19] J. Adeoye, J. A. Omoleye, and M. A. Ojewumi, "Synthesis of zeolite Y from kaolin using novel method of dealumination," *International Journal of Applied Engineering Research*, vol. 12, no. 5, pp. 755–760, 2017.

[20] C. Faizul and C. Abdullah, "Zeolite synthesis from oil palm ash using hydrothermal treatment," *Advanced Materials Engineering and Technology AIP Conference Proceedings*, vol. 1835, Article ID 020016, 2017.

[21] C. P. Faizul, C. Abdullah, and B. Fazlul, "Synthesis of zeolites from treated oil palm ash," *Applied Mechanics and Materials*, vol. 754-755, pp. 1035–1039, 2015.

[22] S. R. Pouya, H. Shafaghat, and M. A. Wan, "Aromatic hydrocarbon production by catalytic pyrolysis of palm kernel shell waste using a Bi-functional Fe/HBeta catalyst: effect of

lignin derived phenolics on zeolite deactivation," *Green Chemistry*, vol. 18, no. 6, pp. 1684–1693, 2016.

[23] Y. Prawiyanto, A. Shofiyani, and T. A. Zaharah, "Synthesis and characterization of zeolite materials from power plant fly ash," *Asian Journal of Chemistry*, vol. 30, no. 5, pp. 993–997, 2018.

[24] N. Salahudeen and A. S. Ahmed, "Synthesis of hexagonal zeolite Y from Kankara kaolin using a split technique," *Journal of Inclusion Phenomena and Macrocyclic Chemistry*, vol. 87, no. 1-2, p. 149, 2016.

[25] V. S. Somerset, L. F. Petrik, R. A. White, M. J. Klink, D. Key, and E. I. Iwuoha, "Alkaline hydrothermal zeolites synthesized from high SiO2 and Al2O3 co-disposal fly ash filtrates," *Fuel*, vol. 84, no. 18, pp. 2324–2329, 2005.

[26] W. K. Sung, S. K. Bon, and H. L. Dong, "Catalytic pyrolysis of palm kernel shell waste in a fluidised bed," *Bioresource Technology*, vol. 167C, pp. 425–432, 2014.

[27] Y. Zarina, A. M. MustafaAl Bakri, H. Kamarudin, I. Khairul Nizar, and A. R. Rafiza, "Review on the various ash from palm oil waste as geopolymer material," *Reviews on Advanced Material Science*, vol. 34, pp. 37–43, 2013.

[28] R. Mallada, "Hydrothermal synthesis of zeolite," in *Encyclopedia of Membranes*, E. Drioli and L. Giorno, Eds., Springer, Berlin, Germany, 2014.

[29] S. Brunauer, P. H. Emmett, and E. Teller, "Adsorption of gases in multimolecular layers," *Journal of the American Chemical Society*, vol. 60, no. 2, pp. 309–319, 1938.

[30] B. Y. Lim, S. Husseinsyah, and P. L. Teh, "A study on the rheological properties of low-density polyethylene/palm kernel shell composites," *Advanced Materials Research*, vol. 626, pp. 615–619, 2012.

[31] A. L. Iskander, E. M. Khald, and A. S. Sheta, "Zinc and manganese sorption behavior by natural zeolite and bentonite," *Annals of Agricultural Sciences*, vol. 56, no. 1, pp. 43–48, 2011.

[32] E. M. Flanigen, R. W. Broach, and S. T. Wilson, *Zeolites in Industrial Separation and Catalysis*, WILEY-VCH, Weinheim, Germany, 2010, ISBN: 978-3-527-32505-4.

[33] M. W. Munthali, A. E. Mohammed, E. Johan, and N. Matsue, "Proton adsorption selectivity of zeolites in aqueous media: effect of Si/Al ratio of zeolites," *Molecules*, vol. 19, pp. 20468–20481, 2014.

[34] R. Wan Nik, *Fluid Catalytic Cracking Handbook*pp. 87–115, Butterworth-Heinemann, Oxford, UK, Third edition, 2012.

[35] M. A. Keane, "Catalytic processing of waste polymer composites," *Management, Recycling And Re-Use Of Waste Composites*, pp. 122–151, Woodhead Publishing Series, Amsterdam, Netherlands, 2010.

[36] P. Chindaprasit, R. Kanchancha, A. Sathonsaowaphak, and H. T. Cao, "Sulfate resistance of blended cements containing flyash and rice husk ash," *Construction and Building Materials*, vol. 21, pp. 1356–1367, 2007.

[37] J. Guo and Z. Ji, "Superhydrophilic ZSM-5 zeolite-coated membrane for enhancing water coalescence in water-in-oil emulsions," *Colloids and Surfaces A: Physicochemical and Engineering Aspects*, vol. 595, p. 124727, 2020.

[38] S. M. Mak, B. T. Tey, K. Y. Cheah, W. L. Siew, and K. K. Tan, "The effect of mechanical grinding on the mesoporosity of steam-activated palm kernel shell activated carbons," *Journal of Chemical Technology & Biotechnology*, vol. 84, no. 9, pp. 1405–1411, 2009.

[39] X. Wang, W. Liu, and Q. Huang, "Simultaneously demulsification and coalescence deoiling of O/W emulsion by a zeolite composite material," *Chemical Engineering and Processing-Process Intensification*, vol. 153, p. 107954, 2020.

[40] N. S. Ahmedzeki and B. A. Al-tabbakh, "Synthesis and characterisation of nano-crystalline zeolite Y," *Al-Khwarizmi Engineering Journal*, vol. 12, no. 1, pp. 78-79, 2016.

[41] N. Taufiqurrahmi, A. R. Mohamed, and S. Bhatia, "Nanocrystalline zeolite Y: synthesis and characterisation," *IOP Conference Series: Materials Science and Engineering*, vol. 12, 2011.

[42] N. Yalcin and V. Sevinc, "Studies of the surface area and porosity of activated carbons prepared from rice husks," *Carbon*, vol. 38, pp. 1943–1945, 2000.

[43] D. J. C. Yates, "Studies on the surface area of zeolites as determined by physical adsorption and X-ray crystallography," *Canadian Journal of Chemistry*, vol. 46, p. 1965, 1968.

[44] M. Greenbank and S. Sports, "Effects of starting material on activated carbon characteristics and performance," *Information Bulletin IB-1017-06/95*, pp. 1–13, Calgon Corporation, Pittsburgh, PA, USA, 1995.

[45] J. G. Martinez, M. Johnson, J. Valla, K. Li, and J. Y. Ying, "Mesostructured zeolite Y-high hydrothermal stability and superior FCC catalytic performance," *Catalysis Science & Technology*, vol. 2, no. 5, pp. 987–994, 2012.

[46] K. S. W. Sing, D. H. Everett, R. A. W. Haul, L. Moscou, R. A. Pierotti, and J. Rouquerol, "Reporting physisorption data for gas/solid systems with special reference to the determination of surface area and porosity (Recommendations 1984)," *Pure and Applied Chemistry*, vol. 57, no. 4, pp. 603–619, 1985.

Hindawi
International Journal of Chemical Engineering
Volume 2020, Article ID 8818224, 8 pages
https://doi.org/10.1155/2020/8818224

Research Article

Fractography and Tensile Properties of AA6061 Aluminium Alloy/ Rice Husk Ash Silicon Nanocomposite

N. E. Udoye,[1] O. S. I. Fayomi,[1,2] and A. O. Inegbenebor[1]

[1]*Department of Mechanical Engineering, College of Engineering, Covenant University, Ota, Ogun State, Nigeria*
[2]*Department of Chemical, Metallurgical and Materials Engineering, Tshwane University of Technology, Private Bag X680, Pretoria 0001, South Africa*

Correspondence should be addressed to N. E. Udoye; nduka.udoye@covenantuniversity.edu.ng

Received 22 May 2020; Revised 17 July 2020; Accepted 12 August 2020; Published 28 August 2020

Academic Editor: Rotimi Sadiku

The unstoppable quest for low-cost reinforcing agent gingered the enthusiasm towards developing and utilising the agro-based waste product as reinforcement since they are promptly accessible, sustainable, and inexpensive to purchase. In this study, AA6061/rice husk ash matrix composites were produced through metallurgical stir casting techniques. Different weight percentages of reinforcement in the range of 2%, 4%, 6%, and 8% were used to fabricate the composites. The reinforced composites were characterized by SEM/EDS for microstructural study. The mechanical behaviour was examined for all the produced samples. SEM/EDS analysis revealed the presence of silica, a major constituent of rice husk ash in the produced composites. The results of the mechanical behaviour show that upgrading the weight percentage of reinforcing agent increases the mechanical properties. AA6061/8% rice hush ash generated a consistent rise with filler concentration in comparison with the aluminium alloy in all operating functions.

1. Introduction

The high cost of ceramic material prompts the use of eco-friendly inexpensive agro-based waste reinforcing materials on aluminium-based alloys for industrial application [1, 2]. The utilization of modern technologies for reducing severe failures in major engineering component is necessary for metal construction industries as a result of its innovative qualities, and studies have revealed that aluminium alloy is the cheapest and global valuable materials [3, 4]. Aluminium alloy is a class of aluminium with low density, light weight, ultimate tensile strength, and hardness [5, 6]. The high demand for aluminium applied in the different application is unquantifiable to the implementation of other metals. Moreover, aluminium is utilized in numerous fields, starting from building construction to kitchen wares. Aluminium and its alloys are applied in numerous factories as a result of their encompassing properties such as higher strength-to-weight ratios, decent corrosion resistance, and exceptional workability [7]. The production of aluminium is invariably broad as it embraces different stages of the metallurgical path. The quest to create cheaper materials, particularly metal matrix composites (MMCs) with enriched structures, has occupied the attention of many researchers [8, 9]. Pure aluminium cannot be used for structural applications except when other elements are included in the substance to obtain sufficient strength for the production of structural members [10]. MMCs are utilized immensely in industrial processes involving light weight with stiffness, superspecific strength, ductility, and resistance due to heat [11]. Fly ash, fibres, whiskers, and particles are few examples of agro-based waste particulate used recently for reinforcement [12, 13]. Numerous researchers desire to use cheaper materials to reinforce aluminium alloy, particularly metal matrix composite with superior properties [14]. However, AA6061 alloy has rough particles and enormous needle/plate-like eutectic silicon, which resulted in low mechanical behaviour. AA6061 alloys are a cluster of Al-Si-Mg and their rises in strength are by the processing of Mg_2Si in the aluminium alloy [10]. The enthusiasm in the improvement of metal

matrix composites (MMCs) is anchored on its mechanical applications for light materials with a unique quality, malleability, and thermal resistance [15]. The desire to produce inexpensive smart composite necessitates numerous inventions in the technological world. Among the several reinforcements used like silicon carbide and aluminium oxide, rice husk ash is the lowest reinforcement attainable in huge quantity as an agro-based waste [16, 17]. Rice husk ash (RHA) was selected because of inherent composition such as silicon embedded in the material. Silicon has high melting and boiling points of 1414°C and 3265°C, which contributed to reducing the melting temperature of the produced composites.

In the current study, the use of AA6061/RHA composites to boost the structural properties of the material was determined. Senapati et al. explore the use of agro-based discarded RHA and fly ash to strengthen the aluminium alloy used in the manufacturing industry. The author deduced that the addition of fly ash and rice husk particulates in the aluminium alloy advances the matrix hardness and the wear properties of the composite [18]. Prasad and Krishna examined the mechanical features of AA356.2/RHA composites. The authors observed more anticipated surface morphology and mechanical characteristics than the as-received sample. The result depicts that the presence of RHA particles leads to the improvement in hardness and strength of the developed composite [2]. Subrahmanyam et al. carried out inoculation of aluminium alloy using agricultural waste rice husk ash. The authors observed that the mechanical properties of MMCs performed better with the inclusion of RHA in aluminium alloy. The microstructure with 8% RHA particles has exceptional mechanical properties and uniformly distributed particulates [19].

According to Haque et al., "the production of inexpensive metal matrix composites strengthened with eco-friendly material has contributed to revolutions in the field of engineering to limit environmental pollution". The authors fabricated and characterized the reinforcement of AA356.2 alloy with RHA particulates. The microstructure study reveals homogeneous dispersal of RHA particulates in the produced composites. Furthermore, it shows that the toughness measured by impact test increases as RHA content increases. It was affirmed that AA356.2/RHA composites could be utilized where light-weight materials are needed with better stiffness and strength [20].

Valyakala et al. studied the source of the destruction of a forced draft fan based on a study carried out in the petrochemical industry. The major factor affecting the failure rate of forced draft fan in a petrochemical industry was vibration, and vibration in turn caused bearing failure. The causes of failure of the fan blade are divided into four main parts: machine, material, equipment, and labour. The authors affirmed that suspended particles in the air instigate erosion on the blades. Therefore, the authors concluded that forced draft fan damage was caused by bearing damage, and it can be evaded by eliminating disruption in the impeller and misalignment of base and fastener failure [21]. Kushwaha studied failure analysis and technique of averting fracture in the generator's fan blade. The authors concluded that the blade crack was due to fatigue situations in resonance state and the growth of existing small feasible cracks [22].

The research complications envisaged are the deformations of machine parts due to environmental generated failure altering the grain borderline. The study provides agro-based waste to boost aluminium alloy in the manufacturing industries. The study aimed to determine the fractography and tensile properties of AA6061 aluminium alloy/rice husk ash silicon nanocomposite to curb the constant failure of equipment in the industry.

2. Materials and Methods

2.1. Matrix Material. The matrix material used in this work is aluminium 6061. Aluminium 6061 is an alloy of aluminium whose main alloying elements are magnesium and silicon. This material is made use of in this work because of the mechanical properties it exhibits, such as strength and good welding ability. In the present study, the chemical composition of the matrix is shown in Table 1.

2.2. Reinforcement Materials. In this study, the reinforcement material is rice husk ash. It is made from rice mill plant in Abakaliki, Ebonyi State. The RHA is cleaned with water to exclude the dust and dehydrated at room temperature for one day. Washed rice husk is then heated to 200°C for one hour to get rid of the moisture. It is then heated to 600°C for 12 h to eradicate the carbon content. The chemical element of RHA is shown in Table 2. Figure 1 shows the flowchart for the processing of rice husk ash.

2.3. Mechanical Properties. Mechanical properties for prepared composites of varying reinforcements were assessed in hardness and tensile properties. The Brinell hardness was measured at a load of 100 g for 15 seconds. The universal testing machine (UTM) SM1000 was used in this work for testing the material tensile strengths.

2.4. Preparation of Composite Samples. The production of AA6061/rice husk ash was done effectively by stir casting method. The study was carried out at different percentage compositions of reinforcement. Firstly, AA6061 is poured into the red heated electrical furnace and the temperature is raised to 750°C until total melting. Slag is extracted to generate good quality of the melt. The obtained RHA is preheated to 600°C in a detached oven and maintained for 20 minutes to eradicate moisture content. The picture of the stir cast arrangement is shown in Figure 2. The mechanical stirrer is dipped into the melt and slowly stirred to create a vortex. Then the preheated rice husk ash is poured to the melt at a temperature of 720°C.

Concurrently, the stirring preparation is taken and transferred at a temperature of 650°C into the preheated moulds of 250 mm × 25 mm size cylindrical hole instantly. Precaution is ensured for the thorough conversion of the molten metal to solid. Figure 3 shows the developed composite material before the tensile test.

Table 1: Chemical composition of AA6061 (wt. %).

Element	Al	Mg	Si	Fe	Cu	Zn	Mn	O
Composition	85.0	3.3	2.25	2.13	1.5	0.25	0.12	5.0

Table 2: Chemical element of RHA reinforcing filler (wt. %).

Constituents	SiO_2	Al_2O_3	Fe_2O_3	CaO	MgO	Na_2O	K_2O
(wt. %)	81.05	12.1	0.98	0.58	1.98	0.06	3.25

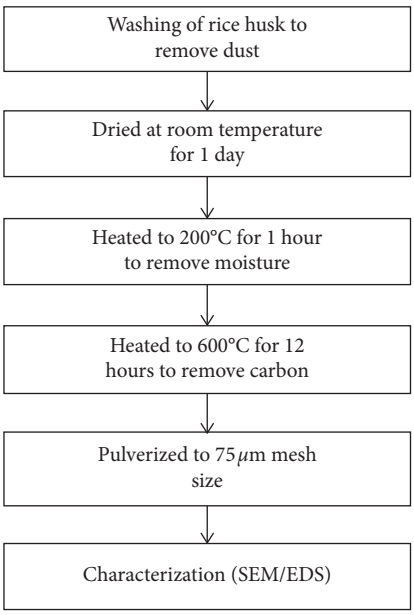

Figure 1: The flowchart for the processing of RHA.

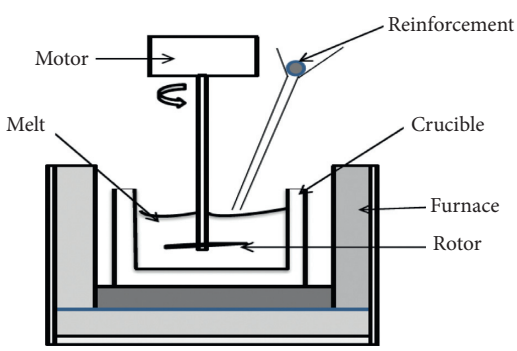

Figure 2: Stir casting technique for the fabrication MMCs.

3. Equipment

3.1. Hardness Testing. The Brinell hardness experiment was done using a 10 mm steel ball indenter TQ SM1000 universal testing machine, the tiny circular specimens were placed in a cavity connected to the axis as a steel ball indenter, and then the steel ball using a lever having hydraulic energy is pushed into the sample for 10 s observation and continued reading the applied force on the digital readout screen. The diameter of the indentation on the samples was determined in a granule consisting of a magnifying glass having a weighing scale. The Brinell hardness value was based on the Brinell scale formula as follows:

Figure 3: Developed composite material before the tensile test.

$$\mathrm{HBS} = \frac{2F}{\pi D\left(D - \sqrt{D^2 - d^2}\right)}, \quad (1)$$

where HBS = H (hardness), B (Brinell), S (steel), F = applied force, D = diameter of indenter, and d = diameter of indentation [23].

3.2. Universal Material Testing Machine. The SM1000 Universal Test Machine Cap 100 kN (10 ton) is used to determine the tensile strength of the developed composites. It is a universal test machine (UTM) commonly known as the universal tester. It is very versatile as it was used to perform the tensile strength tests. This is a multifunctional tensile and hardness testing machine.

3.3. Scanning Electron Microscope (SEM). The scanning electron microscope (SEM) was used to perform the microstructural examinations and phase analysis for each reinforced sample. The microscope is reinforced by an energy dispersion spectrometer (EDS) to determine the quantified composite identity of the elements present in the working samples. For unified elementary research, the TESCAN scanning electron instrument enables high vacuum resolution separation.

4. Results and Discussion

4.1. Morphology Study of AA6061/Rice Husk Ash Reinforcement. Figure 4 shows the SEM/EDS of as-received sample depicting the significant presence of aluminium from the EDS analysis. Figure 5 shows the microstructure of the developed composite prepared by stir casting methods. A homogeneous dispersal of RHA is noticed visibly in Figure 5(b) without cavities and gaps. Figure 6(b) shows the presence of eutectic silicon α-Al phase precipitation and uneven

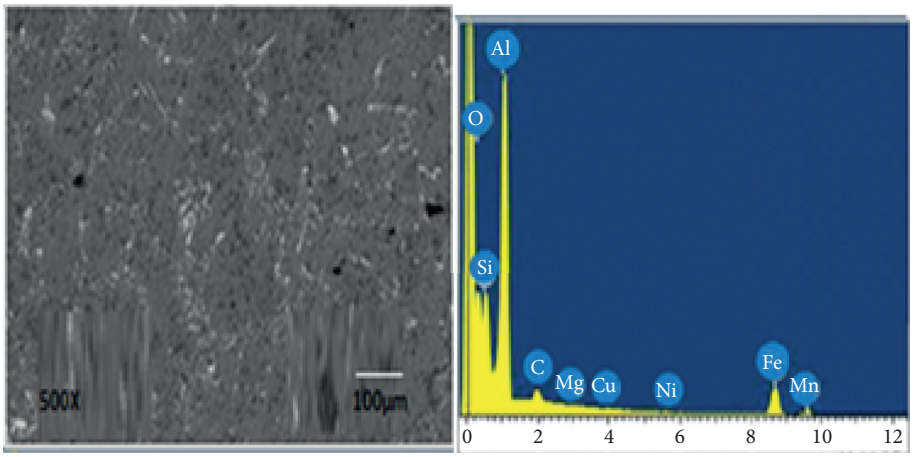

Figure 4: SEM/EDS spectra for as-received AA6061.

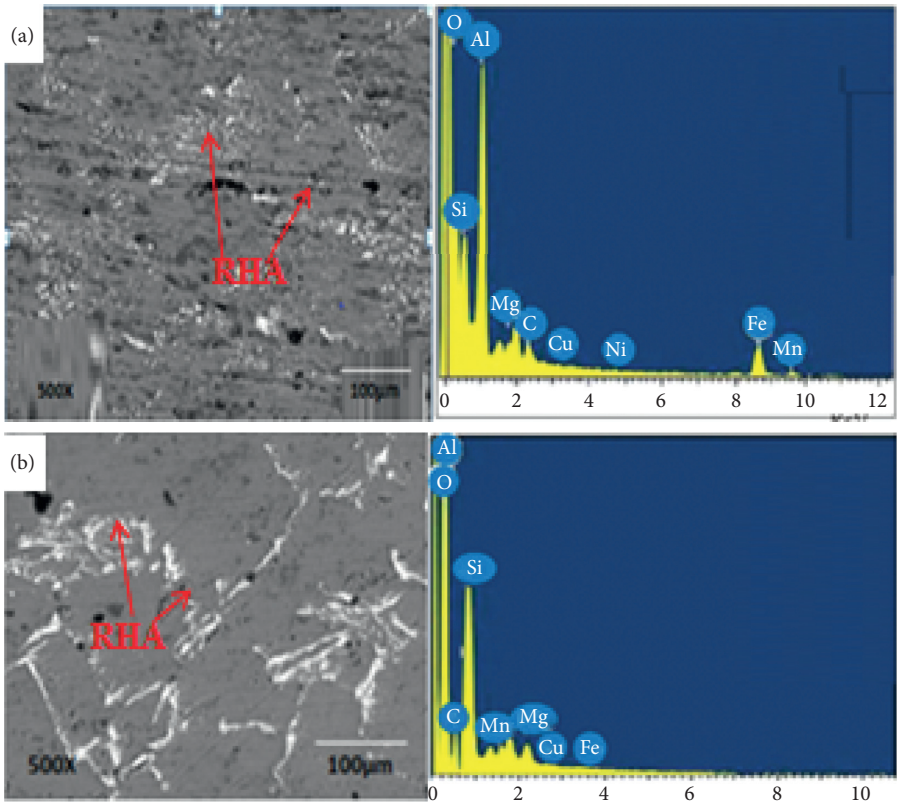

Figure 5: SEM micrograph showing (a) AA6061/2% RHA at 75 μm and (b) AA6061/4% RHA at 75 μm.

distribution of particulate grain refiners. More developed and uniform dispersal of particulates is observed for the sample AA6061/8% RHA at 75 μm. It was noticed that a needle-like particle with well-structured crystal due to the improved arrangement of the reinforcement existed with the elemental composition of all basic collections seen at the EDS. It is interesting to note that the percentage of reinforcements plays a vital role in the stable modification of crystal. In this work, studies by Saravanan and Kumar stated that prospective ceramics particles have an intensity to cause consistent growth due to the nucleation system as seen in Figure 6(b) [24]. Siddharth and Rao stated that the addition of reinforcing agent led to the building of the silica-rich layer at the matrix margin [25].

4.2. Fractured Surface Analysis of AA6061/RHA Composite. The fractured surfaces of the tensile specimens were examined using a scanning electron microscope (SEM), which gives the fracture propagation of the tensile specimens, and Figure 7 shows the fractured SEM image of the starting material. It revealed a flat fracture surface consisting of small fracture facets and tear ridges in the microstructure

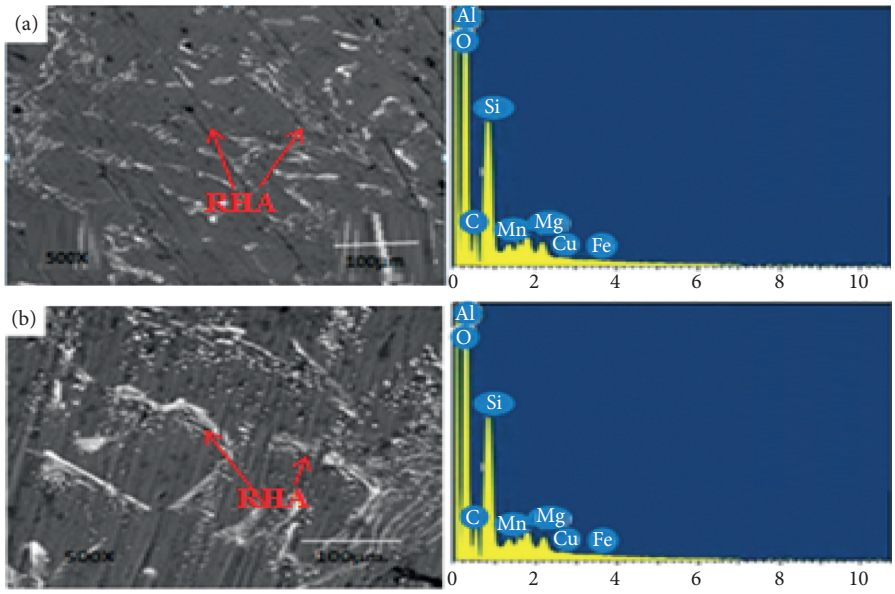

Figure 6: SEM micrograph showing (a) AA6061/6% RHA at 75 μm and (b) AA6061/8% RHA at 75 μm.

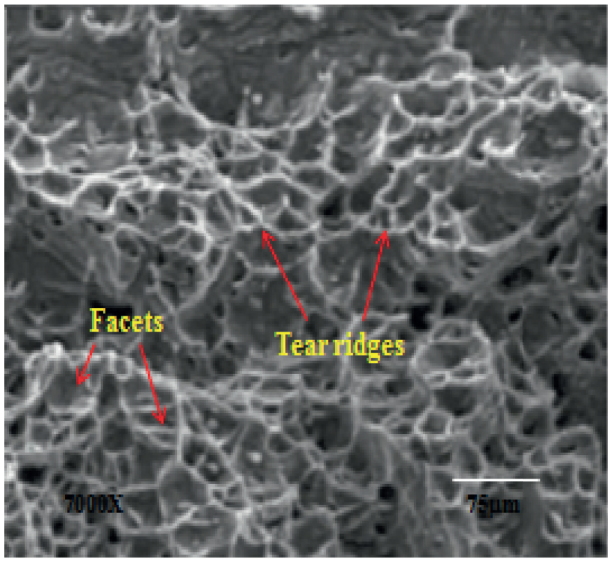

Figure 7: Fractography images of the starting material.

images of the starting material indicating that it is a ductile fracture. Figure 8(a) illustrates the detailed fracture surface morphologies of AA6061/2% RHA composites. The fractured SEM images show a flat fracture surface involving wear track and tear ridges. Maleque et al. stated that fracture occurs in composite material by crack initiation which followed immediately at the boundary between aluminium alloy and reinforcement, and the ductile properties are characterized by the wear track and tear ridges observed on the fractured surface [26].

Figure 8(b) shows the fractography of AA6061/4% RHA composites. It can be observed to have irregular tear ridges and less ductile failure due to more voids and fewer depths of dimple before reinforcements. Figure 8(c) shows the fractography analysis of AA6061/6% RHA composites. It revealed a noticeable dimple effect of the fracture surface, which specifies the ductility of the material. Figure 8(d) shows that AA6061/8% RHA has a higher tensile strength than the as-received sample because of the ductile nature of the material. However, AA6061/8% RHA reveals a noticeable fracture surface after tensile tests in macroscopic images and equal deep dimples spread over the fracture surface. Dimples enclose the greater area with considerable dimple depth and intermetallic segregation which is due to the reinforced agent present in the matrix [27, 28].

4.3. Evaluation of Mechanical Behaviour

4.3.1. Microhardness Analysis of RHA Reinforced AA6061.

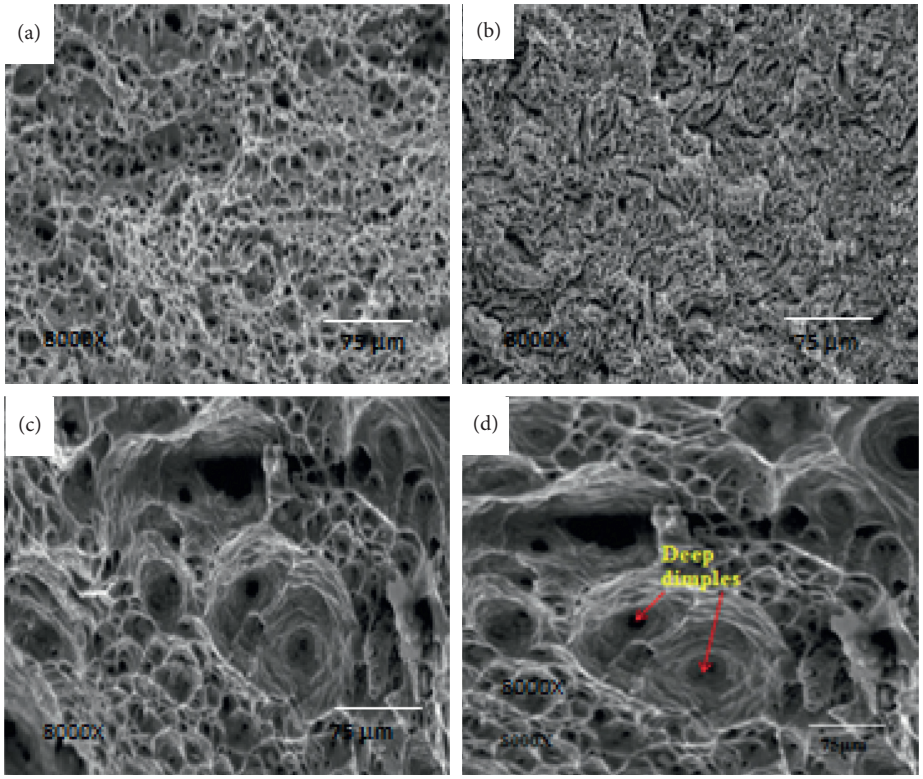

Figure 8: SEM after fracture of (a) AA6061/2% RHA at 75 μm, (b) AA6061/4% RHA at 75 μm, (c) AA6061/6% RHA at 75 μm, and (d) AA6061/8% RHA at 75 μm.

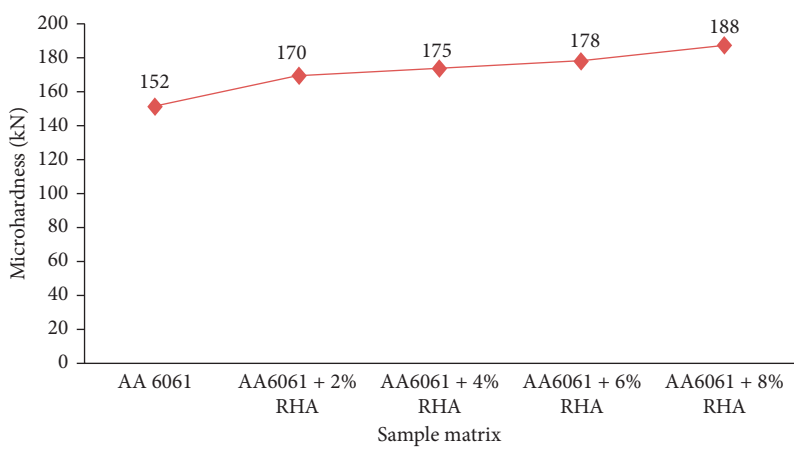

Figure 9: Effect of RHA content on microhardness.

Figure 9 represents the microhardness plot and variable pattern of the reinforced alloys for AA6061/RHA alloy in 75 μm grain sizes. From the obtained data, the fabricated alloys increased linearly in hardness from 152 BHN to approximately 188 BHN at a percentage increment of 23.7%. For critical comparison of the reinforced matrixes, AA6061/8% RHA at 75 μm amidst all others gave a better hardness. Apasi et al. stated that the result of the hardness increase of the alloy composite is seen to be similar to other experiments conducted by the author [29].

4.3.2. Ultimate Tensile Strength for RHA Reinforced AA6061. Figure 10 shows the UTS trend and variable design of reinforced alloys for AA6061/RHA alloy in 75 μm grain sizes. The UTS of the reinforced aluminium MMCs increased significantly from 6000 kPa starting aluminium alloy to approximately 6339 kPa for the developed alloy at a performance influence of 5.65%. For an accurate evaluation of the reinforced matrixes, AA6061/8% RHA at 75 μm amidst all others gave a superior ultimate tensile strength. Gupta and Takhi stated that the higher the percentage of

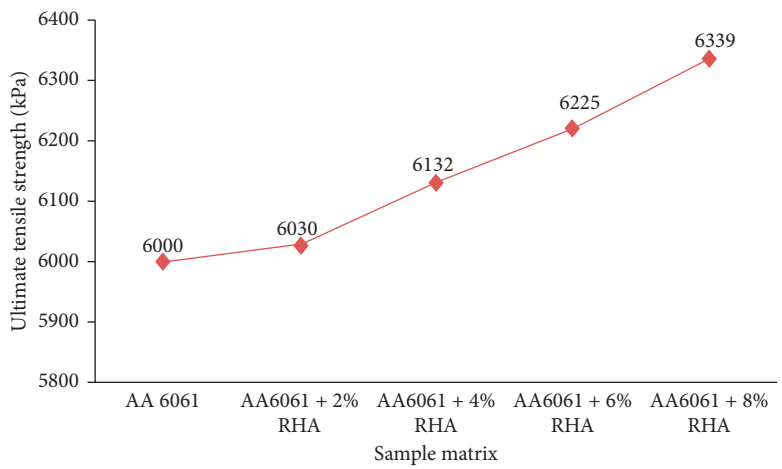

Figure 10: Effect of RHA particles on tensile strength.

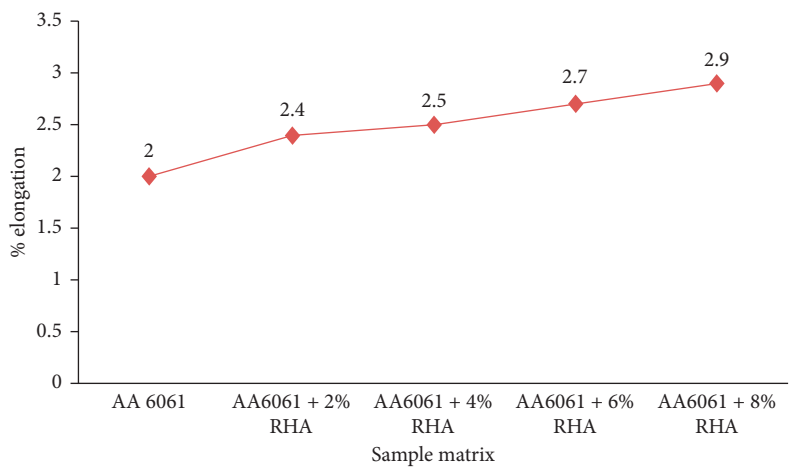

Figure 11: Effect of RHA particles on percentage elongation.

RHA added to the matrix, the higher its tensile strength, thereby causing a boost in the mechanical properties [30].

4.3.3. Elongation Result for Reinforced Aluminium Matrix. Figure 11 shows the percentage elongation analysis and variable influence of the reinforced alloys for AA6061/RHA alloy in 75 μm grain sizes. From the compared process parameter, AA6061 + 8% RHA at 75 μm among the others gave a better superior percentage elongation than the as-received sample. It is noticed that the elongation of composite reduced with the reduction in the percentage of the reinforcement [7].

5. Conclusion

The following conclusions were made:

Agro-based waste rice husk ash particulate can be utilized for the production of MMCs for industrial applications.

AA6061 was successfully reinforced with rice husk through a liquid metallurgy stir casting route.

AA6061/8% RHA gives the maximum tensile value of 6339 kPa in comparison with the 6000 kPa for the as-received sample in all operating conditions.

The developed metal matrix agro-refiner alloy greatly improved the hardness from 152 BHN to 188 BHN at a performance influence of 23.7%.

Data Availability

The data used to support the findings of this study are included within the article.

Conflicts of Interest

The authors declare that there are no conflicts of interest.

Acknowledgments

The authors acknowledge Covenant University for the financial support offered for the publication of this research.

References

[1] K. K. Alaneme, T. M. Adewale, and P. A. Olubambi, "Corrosion and wear behaviour of Al-Mg-Si alloy matrix hybrid composites reinforced with rice husk ash and silicon carbide," *Journal of Materials Research and Technology*, vol. 3, no. 1, pp. 9–16, 2014.

[2] D. S. Prasad and A. R. Krishna, "Fabrication and characterization of AA356.2-Rice husk ash composite using stir casting technique," *International Journal of Engineering Science and Technology*, vol. 2, no. 12, pp. 7603–7608, 2010.

[3] G. Wang, L. Zhu, H. Liu, and W. Li, "Zinc-graphite composite coating for anti-fouling application," *Materials Letters*, vol. 65, no. 19-20, pp. 3095–3097, 2011.

[4] Z. F. Lin, X. B. Li, and L. K. Xu, "Electrodeposition and corrosion behavior of zinc–nickel films obtained from acid solutions: effects of TEOS as additive," *International Journal Electrochemical Science*, vol. 7, pp. 12507–12517, 2012.

[5] N. E. Udoye, O. S. I. Fayomi, and A. O. Inegbenebor, "Assessment of wear resistance of aluminium alloy in manufacturing industry-a review," *Procedia Manufacturing*, vol. 35, pp. 1383–1386, 2019.

[6] M. N. Wahab, A. R. Daud, and M. J. Ghazali, "Preparation and characterization of stir cast aluminum nitride reinforced aluminum metal matrix composites," *International Journal of Mechanical and Materials Engineering*, vol. 4, no. 2, pp. 115–117, 2009.

[7] G. Narasaraju and D. L. Raju, "Characterization of hybrid rice husk and fly ash-reinforced aluminium alloy (AlSi10Mg) composites," *Materials Today: Proceedings*, vol. 2, no. 4-5, pp. 3056–3064, 2015.

[8] B. A. Kumar and N. Murugan, "Metallurgical and mechanical characterization of stir cast AA6061-T6-AlNp composite," *Materials & Design*, vol. 40, pp. 52–58, 2012.

[9] O. S. I. Fayomi, O. O. Joseph, I. G. Akande, C. K. Ohiri, K. O. Enechi, and N. E. Udoye, "Effect of CCBP doping on the multifunctional Al-0.5 Mg-15CCBP superalloy using liquid metallurgy process for advanced application," *Journal of Alloys and Compounds*, vol. 783, pp. 246–255, 2019.

[10] M. Abdulwahab, I. A. Madugu, S. A. Yaro, S. B. Hassan, and A. P. I. Popoola, "Effects of multiple-step thermal ageing treatment on the hardness characteristics of A356.0-type Al-Si-Mg alloy," *Materials & Design*, vol. 32, no. 3, pp. 1159–1166, 2011.

[11] O. S. I. Fayomi, A. P. I. Popoola, and N. E. Udoye, "Effect of alloying element on the integrity and functionality of aluminium-based alloy," *Aluminium Alloys: Recent Trends in Processing, Characterization, Mechanical Behaviour and Applications (Chapter 13)*, pp. 243–260, 2017.

[12] N. Prasad, *Development & Characterization of Metal Matrix Composite Using Red Mud an Industrial Waste for Wear Resistant Applications*, Thesis National Institute of Technology, Rourkela, India, 2006.

[13] U. Rattanasak, P. Chindaprasirt, and P. Suwanvitaya, "Development of high volume rice husk ash alumino silicate composites," *International Journal of Minerals, Metallurgy, and Materials*, vol. 17, no. 5, pp. 654–659, 2010.

[14] V. K. Sharma, R. C. Singh, and R. Chaudhary, "Effect of flyash particles with aluminium melt on the wear of aluminium metal matrix composites," *International Journal Engineering Science and Technology*, vol. 30, pp. 10–15, 2018.

[15] N. E. Udoye, O. S. I. Fayomi, and A. O. Inegbenebor, "The study on improvement of aluminium alloy for engineering application: a review," *International Journal of Mechanical Engineering and Technology*, vol. 10, no. 3, pp. 541–545, 2019.

[16] J.-h. Peng, X.-l. Tang, J.-t. He, and D.-y. Xu, "Effect of heat treatment on microstructure and tensile properties of A356 alloys," *Transactions of Nonferrous Metals Society of China*, vol. 21, no. 9, pp. 1950–1956, 2011.

[17] R. A. Kumar, A. Devaraju, and S. Arunkumar, "Experimental investigation on mechanical behaviour and wear parameters of tic and graphite reinforced aluminium hybrid composites," *Materials Today: Proceedings*, vol. 5, no. 6, pp. 14244–14251, 2018.

[18] A. K. Senapati, S. K. Sahoo, S. Singh, S. Sah, P. R. Padhi, and N. Satapathy, "A comparative investigation on physical and mechanical properties of MMC reinforced with waste materials," *International Journal of Engineering and Advanced Technology*, vol. 5, no. 4, pp. 161–168, 2016.

[19] A. P. S. V. R. Subrahmanyam, G. Naresh, and V. Venkatesu, "Microstructure and mechanical properties of rice husk ash reinforced aluminium alloy (A356.2) metal matrix composite," *IOSR Journal of Engineering (IOSRJEN)*, vol. 8, no. 6, pp. 36–42, 2018.

[20] H. Haque, R. Ahmed, M. Khan, and S. Shahriar, "Fabrication, reinforcement and characterization of metal matrix composites (MMCs) using rice husk ash and aluminium alloy (A-356.2)," *International Journal of Scientific and Engineering Research*, vol. 7, no. 3, pp. 2229–5518, 2016.

[21] A. M. Valyakala, J. Dileeplal, and B. Paul, "Root cause analysis for the failure of a forced draft fan in a petrochemical industry," *International Journal of Engineering Research and Development*, vol. 6, no. 5, pp. 84–90, 2013.

[22] T. N. Kushwaha, "Fatigue failure analysis of a cooling fan blade: a case study," *International O and M Conference*, vol. 6, pp. 717–726, 2017.

[23] H. Soares, T. Zucarelli, M. Vieira, M. Freitas, and L. Reis, "Experimental characterization of the mechanical properties of railway wheels manufactured using class B material," *Procedia Structural Integrity*, vol. 1, pp. 265–272, 2016.

[24] S. D. Saravanan and M. S. Kumar, "Effect of mechanical properties on rice husk ash reinforced aluminum alloy (AlSi10Mg) matrix composites," *Procedia Engineering*, vol. 64, pp. 1505–1513, 2013.

[25] D. Siddharth and J. B. Rao, "Synthesis and characterization of RHA (rice husk ash) particulates reinforced A7075 composites," *International Journal of Advances in Mechanical and Civil Engineering*, vol. 4, no. 3, pp. 105–110, 2017.

[26] M. A. Maleque, A. A. Adebisi, and N. Izzati, "Analysis of fracture mechanism for Al-Mg/SiCp composite materials," *Materials Science and Engineering*, vol. 184, no. 1, 2017.

[27] S. Ozden, R. Ekici, and F. Nair, "Investigation of impact behaviour of aluminium based SiC particle reinforced metal-matrix composites," *Composites Part A: Applied Science and Manufacturing*, vol. 38, no. 2, pp. 484–494, 2007.

[28] S. Chandrasekhar, P. N. Pramada, and J. Majeed, "Effect of calcination temperature and heating rate on the optical properties and reactivity of rice husk ash," *Journal of Materials Science*, vol. 41, no. 23, pp. 7926–7933, 2006.

[29] A. Apasi, D. S. Yawas, S. Abdulkareem, and M. Y. Kolawole, "Improving mechanical properties of aluminium alloy through addition of coconut shell-ash," *Journal of Science and Technology*, vol. 36, no. 3, pp. 34–43, 2016.

[30] V. Gupta and S. Takhi, "Effects of rice husk ash particulates on the mechanical and tribological properties of the aluminum metal composite reinforced with aluminum oxide," *International Journal for Scientific Research and Development*, vol. 3, no. 3, 2015.